Magnetic interactions in water based ferrofluids studied by Mössbauer spectroscopy

2007 J. Phys.: Condens. Matter 19 016205

(http://iopscience.iop.org/0953-8984/19/1/016205)

INSTITUTE OF PHYSICS PUBLISHING JOURNAL OF PHYSICS: CONDENSED MATTER

J. Phys.: Condens. Matter **19** (2007) 016205 (16pp) doi:10.1088/0953-8984/19/1/016205

Magnetic interactions in water based ferrofluids studied by Mössbauer spectroscopy

V Kuncser[1,4], G Schinteie[1], B Sahoo[2], W Keune[2], D Bica[3], L Vekas[3] and G Filoti[1]

[1] National Institute for Physics of Materials, PO Box MG 7, 77125, Bucharest-Magurele, Romania
[2] Fachbereich Physik, Universität Duisburg-Essen Lotharstraße 65, D-47048, Duisburg, Germany
[3] Romanian-Academy-Timisoara Branch, Center for Advanced and Fundamental Technical Research, Mihai Viteazal Nr. 23, 300223, Timisoara, Romania

E-mail: kuncser@infim.ro

Received 11 August 2006, in final form 10 November 2006
Published 7 December 2006
Online at stacks.iop.org/JPhysCM/19/016205

Abstract

Various samples of ferrofluids consisting of colloidal suspensions of surfacted cobalt ferrite or magnetite nanoparticles in water were studied by x-ray diffraction and temperature dependent Mössbauer spectroscopy. Information about the particle mean size, the size dispersion and the effective magnetic anisotropy energy was obtained for each sample. The results are consistent with the formation of a magnetic dead layer at the particle surface, whose thickness depends on the surfactant–ferrite combination. The magnetic relaxation processes are faster in the colloidal suspensions of magnetite particles as compared with the suspensions of cobalt ferrite particles. The type of the surfactant also influences the magnetic relaxation behaviour, and hence the macroscopic properties of the ferrofluid at ambient temperature.

(Some figures in this article are in colour only in the electronic version)

1. Introduction

Magnetic fluids show various novel interesting properties. A magnetic fluid, also known as a ferrofluid, is a colloidal suspension of microscopic permanent magnets. Usually, it consists of a solution of a ferro- or ferrimagnetic nanoparticles dispersed in a polar or non-polar carrier liquid, such as water or oil. Their behaviour in a magnetic field leads to many interesting applications, some of them already entering our everyday life. The ferrofluid applications in the sealing technology, in the viscoelasticity, in the heat transfer or in the magnetically controlled thermal flow [1–6] and also in biomedicine [7–9] have to be mentioned. Further applications include printer inks, magneto-rheological fluids and shock absorbers [10, 11].

[4] Author to whom any correspondence should be addressed.

The ferrofluids are conceptually simple materials, as they can be seen in a first approximation as a system of magnetic dipolar hard spheres dispersed in a viscous medium. Most of the applications of the magnetic fluids involve both their hydrodynamic/thermodynamic properties and the magnetic properties of the constituent nanoparticles. The long spatial range of the dipole interactions and the peculiar viscosity of the non-homogenous medium prevent the accurate description of the thermodynamic and hydrodynamic properties of ferrofluids. Additional difficulties can be encountered in strong interacting ferrofluids, because of the agglomeration of the magnetic particles under applied magnetic fields. Further, the low dimensionality of the constituent magnetic nanoparticles provides a peculiar magnetic behaviour of the system, connected with both magnetic relaxation phenomena and their anomalous spin structure at the particle surface. Therefore, the understanding of the magnetic properties of colloidal dispersions of magnetic nanoparticles remains at the forefront of current research.

In order to maintain the stability of the colloidal dispersion, one must avoid the agglomeration of the magnetic nanoparticles, by counterbalancing both the long-range magnetic and the short-range van der Waals forces.

The magnetic interaction energy between two particles is minimum when the particles are in contact, and it is proportional to the square of the magnetization per volume unit and to the particle volume [1]. The long-range magnetic forces are not able to segregate the particles when the magnetic interaction energy is less than the thermal energy, $k_{\mathrm{B}}T$ (with k_{B} the Boltzmann constant and T the temperature). Therefore, the dispersion conditions with respect to the magnetic interaction forces require a small magnetization per unit volume of the ferrofluid and/or particles of small volumes. By contrast, most applications of the ferrofluids involve a high sensitivity to an applied field, and, consequently, a high magnetization per unit volume. On the other side, the magnetic anisotropy energy of the particle can decrease below the thermal energy at ambient temperature, if the volume of the particle becomes too small. Hence, the magnetic system enters the superparamagnetic regime and is not able to respond anymore like a magnet to an external magnetic field, at room temperature. A compromise for the magnetic particle size and the particle magnetic moment is required, in order to minimize the magnetic interactions between particles and also to respond efficiently to the action of an external magnetic field. Typical sizes for magnetic particles in ferrofluids range between 5 and 20 nm. However, particles of such low size are magnetic single domains.

Short range van der Waals attractive forces can be compensated either electrostatically, if the magnetic particles are charged, or sterically, if their surface is coated with surfactants. The surfactants are long-chain polar molecules which adhere to the surface of the particles, thereby preventing agglomeration by entropic repulsion. Steric repulsion is very effective mainly in ferrofluids with non-polar solvents (e.g. oils). The dispersion of ferrite-like magnetic particles in water (a polar solvent) can be ensured by taking additional precautions. A double layer steric combined with an electrostatic repulsion may be used. It has been reported [12] that clusters of nanoparticles could still form in water-based magnetic fluids due to the non-complete cancelling of the interparticle interactions. They appear mainly in magnetic fluids with a high volume fraction of magnetic nanoparticles (the volume fraction of a ferrofluid is defined by the ratio between the total volume of the constituent nanoparticles and the total volume of the system). Typical values are in the range between 0.01 and 0.1. High volume fractions are required for some applications. Values much higher than 0.1 are currently reported [12]. In spite of the possible clustering processes, the net attractive interparticle interactions are expected to be quite weak, due to both the steric repulsion induced by the double coating layers and the small size of the particles. In the following, the attractive interactions are considered to induce only small perturbations of the main magneto-crystalline anisotropy energy of the

Table 1. The characteristics of the four different ferrofluids.

Sample label	Carrier liquid	Particle type	Coating double layer
S1	H_2O	$CoFe_2O_4$	Myristic acid + myristic acid
S2	H_2O	Fe_3O_4	Myristic acid + DBSA
S3	H_2O	$CoFe_2O_4$	Oleic acid + oleic acid
S4	H_2O	Fe_3O_4	Lauric acid + lauric acid

particles. Colloidal dispersions of quasi-non-interacting magnetic particles will be supposed for all the analysed systems.

Ferrite-like nanoparticles in a ferrofluid can magnetically relax by two different relaxation mechanisms: (i) the Néel relaxation, which is characterized by the thermally activated internal reorientation of the magnetization against an internal energy barrier, and (ii) the Brownian relaxation due to the rotational diffusion of the particles (seen as magnetic dipoles) in the liquid. The effective relaxation depends on the dominant relaxation process. There is no initially known relation between the two specific relaxation times. They depend on many internal parameters as well as on the size of the magnetic particle and are often competing processes. A way to separate the two contributions, for a correct interpretation of the experimental results, is to cut off one of the two components by choosing suitable experimental conditions. For example, the Brownian relaxation can be removed by freezing the magnetic liquid at low temperatures. Temperature dependent Mössbauer spectroscopy can be applied in this situation, providing information on particle phase composition, local structure and symmetry, local magnetic interactions inside the particle and Néel-type relaxation phenomena. This work reports on the magnetic behaviour of ferrofluids consisting of ferrite-like magnetic particles coated with double layers of surfactants and dispersed in water. The influence of the oxide type and of the surfactant layers on the magnetic parameters and the magnetic relaxation regimes is analysed by low-temperature Mössbauer spectroscopy. Additional structural information is obtained by x-ray diffraction techniques. It will be demonstrated that a suitable interpretation of the temperature dependent relaxation phenomena may provide information on the particle size distribution and on either the effective anisotropy constant of the particles or their magnetic volume.

2. Experimental details

Four samples of ferrofluid were prepared by chemical coprecipitation followed by double layer steric and electrostatic stabilization of cobalt ferrite ($CoFe_2O_4$) or magnetite (Fe_3O_4) nanoparticles in water. Details of the preparation can be found in [12]. The four samples, labelled by S1, S2, S3 and S4, are described in table 1.

Samples S1 and S3 consist of nanoparticles of $CoFe_2O_4$ coated by a double layer of myristic acid (S1) and oleic acid (S2), dispersed in water. Samples S2 and S4 consist of Fe_3O_4 nanoparticles coated by a layer of myristic acid and a layer of dodecyl-benzene-sulphonic acid (DBSA) and by a double layer of lauric acid, respectively. The samples were analysed by x-ray diffraction at room temperature (RT) and by ^{57}Fe Mössbauer spectroscopy at temperatures ranging from 4.2 to 250 K. X-ray diffraction (XRD) was performed in the usual θ–2θ geometry by using Cu K_α radiation ($\lambda = 0.154\,06$ nm). Mössbauer spectra were collected in transmission geometry by inserting the sample in a bath liquid-He cryostat. A Mössbauer drive system operating in constant acceleration mode combined with conventional electronics and a ^{57}Co (Rh matrix) source of about 50 mCi activity were employed. The spectra

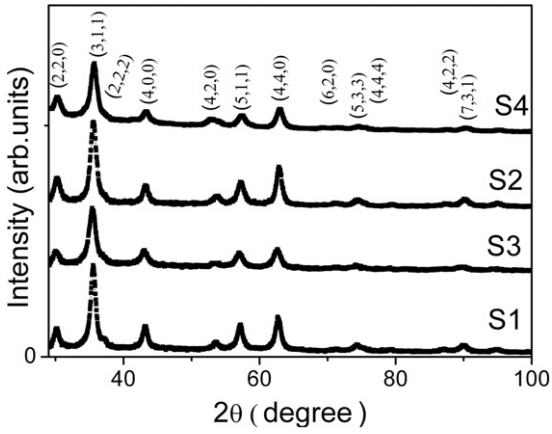

Figure 1. XRD diagrams of samples S1–S4, taken in θ–2θ geometry by using Cu K_α radiation ($\lambda = 0.154\,06$ nm).

Table 2. The lattice parameters and the mean coherence length of the nanoparticles, as deduced by XRD.

Sample	a (nm)	D (nm)
S1	0.845(1)	10.1(8)
S2	0.838(1)	12.1(8)
S3	0.840(1)	11.2(8)
S4	0.835(1)	10.9(8)

were least-squares fitted with the NORMOS computer program, which offers options for both discrete and continuously distributed hyperfine parameters [13]. The isomer shifts are reported relative to α-Fe at room temperature.

3. Results and discussion

3.1. X-ray diffraction

The x-ray diffraction diagrams obtained at room temperature for all the samples investigated are shown in figure 1. Bragg reflections specific to the spinel structure were observed for all samples. The lattice parameter, a, of the cubic structure has been calculated via the Bragg formula:

$$2d \sin\theta = n\lambda \tag{1}$$

with $\lambda = 0.154\,06$ nm, $n = 1$ and the interplanar distance d, dependent on the Miller indices $h, k, l,$, given by

$$\frac{1}{d^2} = \frac{h^2 + k^2 + l^2}{a^2}. \tag{2}$$

According to the above relation, a linear dependence is expected between $\sin^2\theta$ and $(h^2 + k^2 + l^2)$ with the slope equal to $\lambda^2/(4a^2)$ [14]. A plot of $\sin^2\theta$ versus $(h^2 + k^2 + l^2)$ is shown in figure 2(a). At a first view, one can say that the lattice parameter is almost the same for all samples. The accurate fitting procedure with linear dependences leads to the lattice parameters presented in table 2. These values are very close to the value of 0.840 nm reported in the literature [15] for both cobalt ferrite and magnetite structures, proving well crystallized phases inside the nanoparticles.

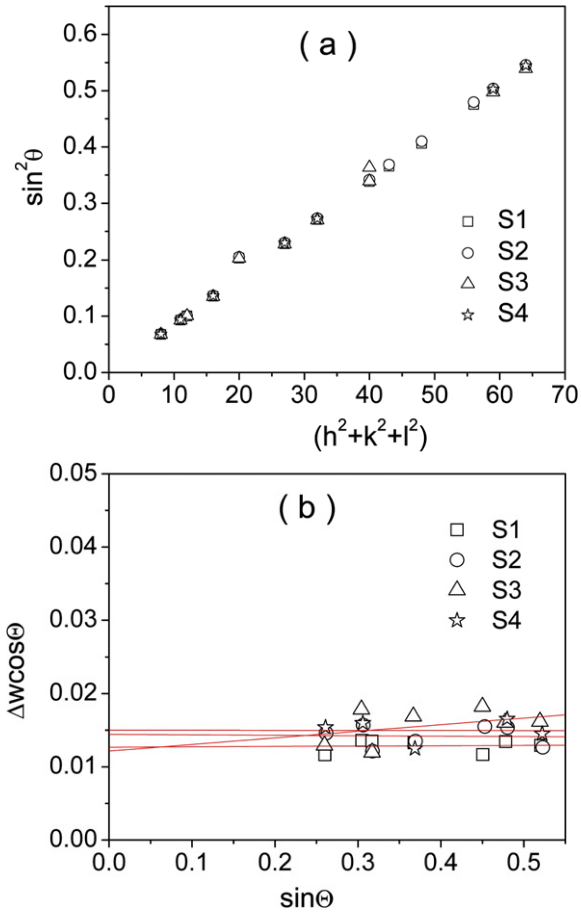

Figure 2. (a) Plot of $\sin^2\theta$ versus $(h^2 + k^2 + l^2)$ for samples S1–S4 (θ is the angular position of the Bragg peak corresponding to Miller indices (h k l)). The lattice parameter of the cubic spinel structure was derived from the slope of the linear fitting of each set of data. (b) Plots of $\Delta W \cos\theta$ versus $\sin\theta$ and their linear fittings for samples S1–S4 (ΔW is the width of the Bragg peak at angle θ). The structural coherence length L was derived from the intersection with the ordinate of the fitted straight line for each sample.

The structural coherence length, L, supposed to approximate the mean particle size, D (D = physical diameter of the nanoparticles, considered as spherical), was obtained via the Scherrer formula from the linear dependence of $\Delta W \cos\theta$ versus $\sin\theta$ [14]:

$$\Delta W \cos\theta = k\lambda/L + \eta \sin\theta \tag{3}$$

with $k = 1$ for spherical particles and η the strain coefficient. ΔW is the linewidth (FWHM) of the diffraction peak at angle θ (the instrumental effects were subtracted). The experimental dependences $\Delta W \cos\theta$ versus $\sin\theta$ for the most pronounced peaks in the XRD diagrams (see figure 2(b)) were analysed by linear fits. The slopes of the straight-line fits were almost insignificant, proving negligible strain contribution to the diffraction linewidths. The mean sizes D of the particles obtained from the intersections of the fitted straight lines with the ordinate are also given in table 2. Accordingly, the physical mean diameter of the particles in the different samples falls in a narrow range between 10.0 and 12.0 nm.

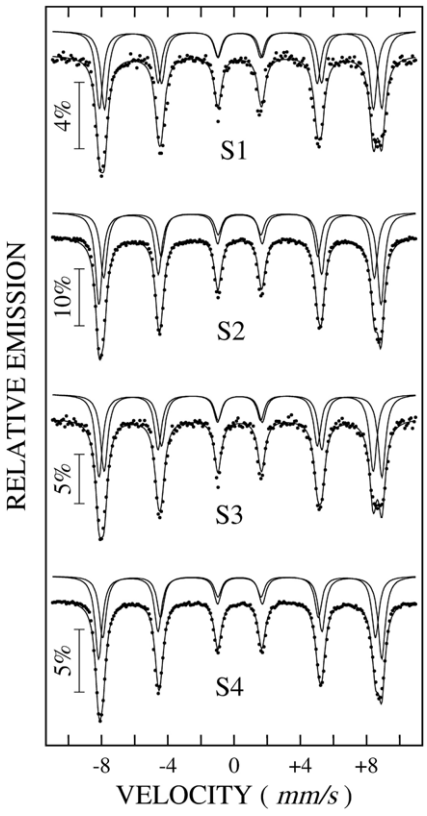

Figure 3. Mössbauer spectra measured at 4.2 K for samples S1–S4 (from top to bottom).

3.2. Mössbauer spectroscopy

The magnetic behaviour of the systems was studied by Mössbauer spectroscopy. Mössbauer spectra collected at 4.2 K are presented in figure 3. They consist in a Zeeman-split-like sextet with an average isomer shift of about 0.43 mm s^{-1} and an average hyperfine field $\langle B_{hf} \rangle$ of about 52 T, typical for spinel ferrites. Known aspects concerning the ferrite structure were considered in order to fit these spectra. The spinel ferrite structure (general formula AB_2O_4) consists in a face centred cubic oxygen (O) array with eight formula units and with divalent or trivalent transition metal cations on the eight tetrahedral (A) and 16 octahedral (B) positions [16]. There are two structural limits: (i) the normal spinel ferrite, when Fe^{3+} ions occupy all the 16 octahedral (B) positions and a divalent transition metal cation, M^{2+}, occupies the eight tetrahedral (B) positions, and (ii) the inverse spinel ferrite, when Fe^{3+} ions occupy all eight tetrahedral (A) positions whereas the 16 octahedral (B) positions are equally shared by Fe^{3+} and M^{2+} cations. In our case, both cobalt ferrite ($CoFe_2O_4$) and magnetite (Fe_3O_4) are typically inverse spinels (Co^{2+} and Fe^{2+} respectively on the B positions).

The magnetic structure of the spinel ferrite is determined by the antiferromagnetic coupling between the magnetic ions on the A and B sites (oxygen mediated super-exchange interactions take place). In this respect, for our compounds, the net magnetic moment per formula unit is due to the spin contribution of the divalent ion on the B site after compensation of the two spins of Fe^{3+} on the A and B sites which are antiparallelly coupled. A slightly higher net magnetic moment is expected for magnetite than for cobalt ferrite because of the higher spin state of Fe^{2+} ($S = 2$) as compared to the spin state of Co^{2+} ($S = 3/2$).

It is very difficult to distinguish between Mössbauer sextets belonging to Fe^{2+} or Fe^{3+} ions or between octahedral or tetrahedral Fe positions in the low-temperature Mössbauer spectra of defect-containing spinel ferrites. Following [16] a much clearer distinction between octahedral and tetrahedral positions can be achieved in bulk magnetite at room temperature, whereas a distinction between Fe^{2+} and Fe^{3+} ions is more evident at low temperature. However, in our case, two subspectra are clearly evidenced in the 4.2 K Mössbauer spectra of the cobalt ferrite nanoparticles where only Fe^{3+} ions are present. Therefore, in order to keep a similar analysis of all samples, the Mössbauer spectra in figure 3 were fitted by two sextet components with the following assignation: one with a higher magnetic hyperfine field, B_{hf}, of about 52.5 T, corresponding to the octahedral sites, and the other one with a lower field of about 51.1 T, corresponding to the tetrahedral sites. Their relative spectral area obtained from the fitting gives a relative contribution of octahedral and tetrahedral Fe-ions of about 1:1 in samples S1 and S3 and of about 2:1 in samples S2 and S4. This is in agreement with the nearly equal occupation of the B and A positions by Fe^{3+} ions in cobalt ferrite, and with the occupation of the B sites by Fe^{3+} and Fe^{2+} ions and of the A sites only by Fe^{3+} ions in magnetite. The large linewidths (above 0.5 mm s^{-1}) of the two sextet components are correlated presumably with defect-associated Fe positions at the surface of the nanoparticles. Our results are consistent with an almost ideal atomic occupation of the inverse spinel structure. Consequently, the Mössbauer spectra at 4.2 K are able to give information on both the type of the spinel used in the ferrofluid, as well as its atomic occupation.

The Mössbauer spectra measured at different temperatures between 4.2 and 250 K are shown in figures 4–7 for samples S1, S2, S3 and S4, respectively. The initially already broad lines of the Mössbauer sextets at 4.2 K for samples S1, S2 and S3 become even broader with increasing temperature. Further, a relaxed central component (10–15% in relative spectral area) develops faster at higher temperatures. By contrast, the Mössbauer sextet of sample S4 rapidly increases its linewidth with rising T and reaches a collapsing regime already at about 175 K.

The above mentioned behaviour of the Mössbauer spectra can be qualitatively described in the frame of the usual magnetic relaxation regimes. The magnetic anisotropy energy of a spherical magnetic particle is KV, with K the magnetic anisotropy energy constant and V the volume of the particle. For nanoparticles of mean dimension below 20 nm, the thermal energy, $k_B T$, can approach the anisotropy energy already at usual temperatures. Therefore, the magnetic properties of an assembly of quasi-non-interacting fine particles are imposed by the thermally driven fluctuations of the magnetic moments of the nanoparticles. It is worthwhile mentioning that at this dimension the nanoparticles are single magnetic domains, and the magnetic entities within the nanocrystals (e.g. the atomic spins) fluctuate coherently [17]. The fluctuation process is identical at the spin (atomic moment) level, as well as for the overall magnetic moment per particle. Therefore, the relaxation process observed by Mössbauer spectroscopy (due to the thermal fluctuation of the Fe spins) can be analysed via the usual theories describing the fluctuation of the overall particle magnetic moment (no external applied magnetic field is required for the Mössbauer study of the relaxation processes and only the temperature must be varied). For a particle with uniaxial anisotropy, the energy $E(\theta)$ required for changing the direction of the total magnetic moment (or the total spin) by an angle θ from the magnetic easy axis is given by

$$E(\theta) = KV \sin^2 \theta. \tag{4}$$

The theoretical treatment of the thermally induced fluctuations is usually divided into two regimes, depending on the ratio $r = k_B T/KV$: (i) the regime of the collective excitations, for $r < 0.1$, and (ii) the regime of the superparamagnetic relaxation, for $r > 0.1$ [17].

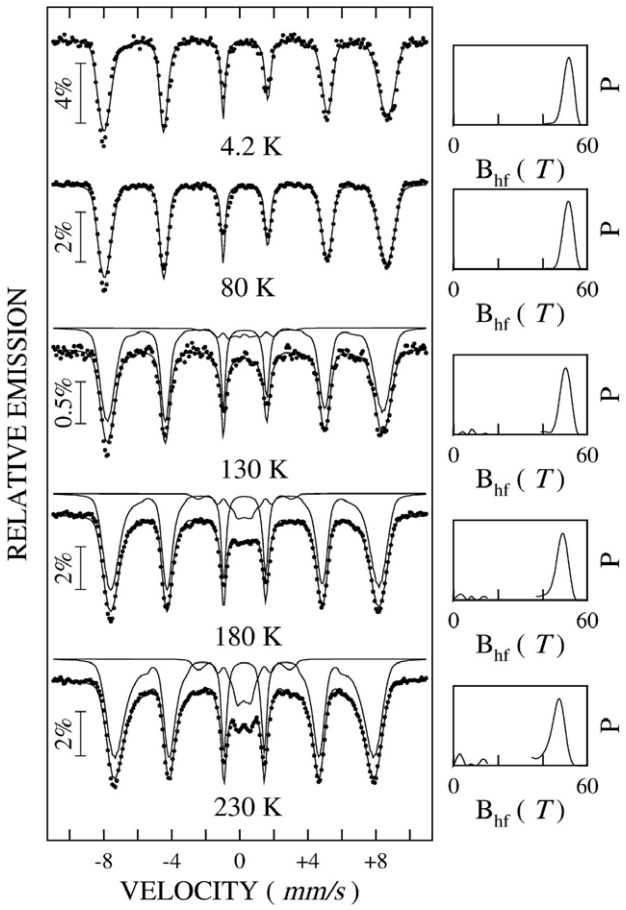

Figure 4. Mössbauer spectra of sample S1 measured at various temperatures. The probability distribution of the magnetic hyperfine field is shown on the right side.

In the regime of collective excitations, the local spins fluctuate by small angles θ around the equilibrium direction (e.g. the magnetic easy axis), leading to an almost linear decrease of the hyperfine field with temperature [17, 18]:

$$B_{\mathrm{hf}} = B_0 \left(1 - \frac{k_{\mathrm{B}} T}{2KV}\right) \tag{5}$$

with B_{hf} the hyperfine field at temperature T and B_0 the hyperfine field in the static regime (e.g. at very low temperature). We suppose that for Fe distributed positions, the above relation (5) may be successfully applied for average hyperfine fields $\langle B_{\mathrm{hf}} \rangle$ and $\langle B_0 \rangle$.

In the superparamagnetic relaxation regime, the spins fluctuate by $\theta = 180^\circ$ along the easy-axis direction with a fluctuation time, τ, given in the simplest form by the Néel model [19]:

$$\tau = \tau_0 \exp(KV/k_{\mathrm{B}}T). \tag{6}$$

The observed spin relaxation process actually depends on the value of τ as compared to the characteristic measurement time of the method, τ_m. If $\tau \ll \tau_m$, the magnetic relaxation appears so fast that the particle system behaves as a paramagnet, with a giant spin per particle (the superparamagnetic regime), whereas for $\tau \gg \tau_m$ the relaxation appears so slow that quasi-static properties are observed (the blocked regime). The temperature at which $\tau = \tau_m$ is defined as the blocking temperature, T_{B}, and, therefore, the value of T_{B} observed depends on τ_m. In spite of the clear phenomenological definition of the blocking temperature, different procedures

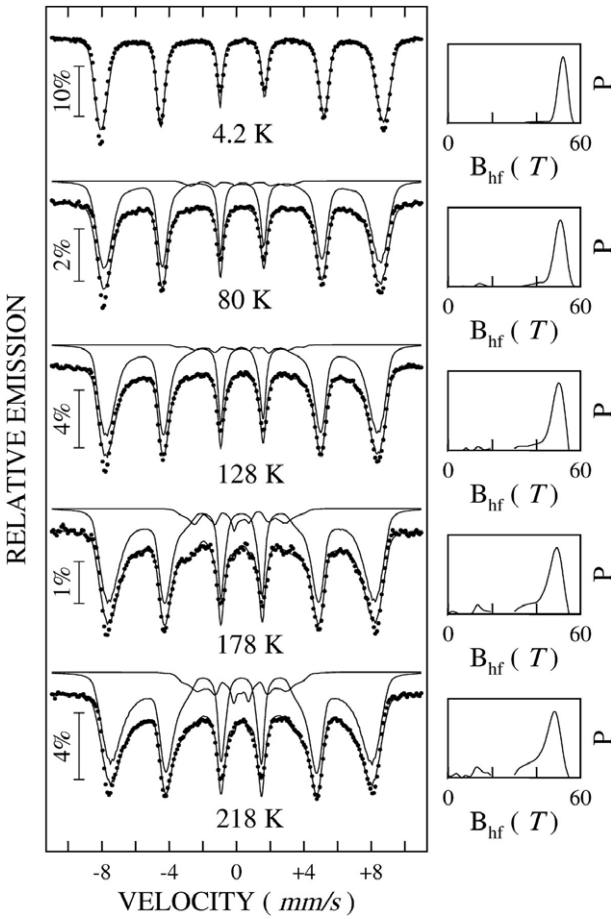

Figure 5. Mössbauer spectra of sample S2 measured at various temperatures. The probability distribution of the magnetic hyperfine field is shown on the right side.

for finding the experimental blocking temperature (where $\tau = \tau_m$) are proposed, depending on the experimental technique. The Mössbauer technique is characterized by a relatively short characteristic measurement time window, τ_M, of the order of $\sim 5 \times 10^{-9}$ s [16, 17]. For a given nano-particle size, the fluctuating time decreases with the temperature according to equation (6), and, consequently, the Mössbauer spectrum presents a magnetic hyperfine field averaged to zero as soon as the spin fluctuation time becomes much shorter than τ_M. Within an appropriate regime of temperatures (corresponding to τ not far away from τ_M) the Mössbauer sextet which characterizes a magnetic site will collapse toward a doublet or singlet. The blocking temperature, as obtained from Mössbauer spectra taken at different temperatures, is usually taken as that temperature where the relative spectral area of the non-collapsed part of the spectrum (sextet) is equal to the relative spectral area of the already collapsed part of the spectrum (doublet or singlet). Large errors in the evaluation of the spectral contribution of the non-collapsed pattern might be introduced due to unsuitable fitting of the collapsing sextets via fitting functions suitable to a static regime.

3.3. Determination of the blocking temperature

We consider, as a more convenient way to find the blocking temperature, T_B, the analysis of the T-dependence of the Mössbauer spectra by a fitting procedure based on distributed magnetic

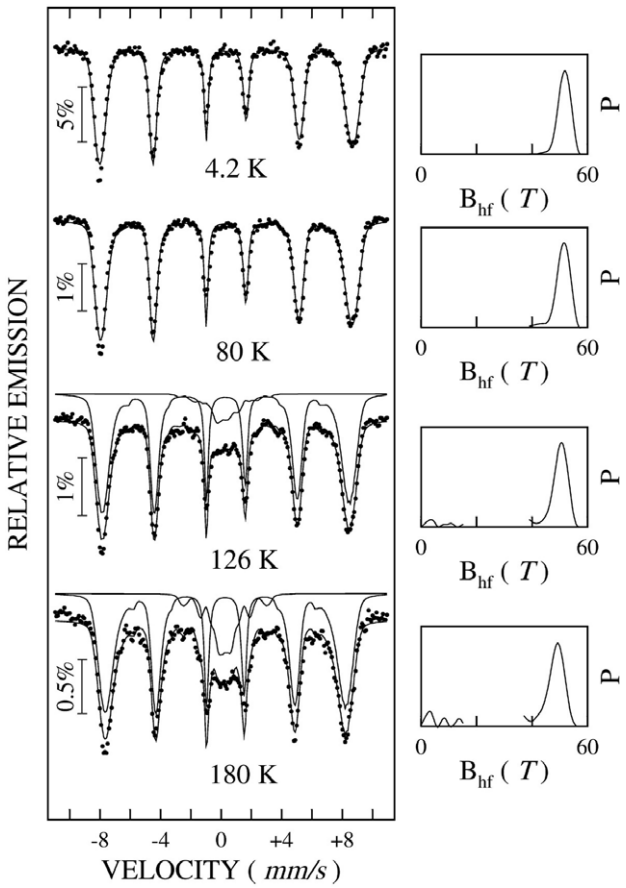

Figure 6. Mössbauer spectra of sample S3 measured at various temperatures. The probability distribution of the magnetic hyperfine field is shown on the right side.

hyperfine fields. It is based on the specific dependence of the effective magnetic hyperfine fields on the relaxation time, and hence on the temperature. This procedure is definitely most adequate in the case of distributed Fe sites, as usually present in nanosized particles. According to this procedure, the Mössbauer spectra at different temperatures are fitted with a distribution of magnetic hyperfine fields. The distribution of hyperfine fields, $P(B_{\mathrm{hf}})$, has to change with temperature due to the specific spin relaxation of Fe atoms at different Fe sites. Therefore, the main information on the magnetic relaxation process should be contained in the typical temperature variation of the hyperfine field distribution (or its associated parameters). A relatively narrow distribution peak centred at a high magnetic hyperfine field is expected in the static and quasi-static regimes. When increasing the temperature, first the peak will become broader and will shift to lower hyperfine fields in a quasi-linear manner, according to the regime of collective excitations. In an intermediate range of temperatures, the distribution $P(B_{\mathrm{hf}})$ will become very broad and mostly structureless due to the onset of the spectral collapse. By increasing the temperature further, the distribution $P(B_{\mathrm{hf}})$ should become narrow again, but with a defined peak at very low magnetic hyperfine fields (close to zero), corresponding to the superparamagnetic (complete relaxation) regime. Correspondingly, we can relate the peak at larger hyperfine fields to the magnetic pattern and the contribution at very low (or zero) fields to the collapsed central component in the spectrum. We propose an alternative definition of the transition from the blocked (low T) to the relaxed (high T) regime, and hence of the blocking

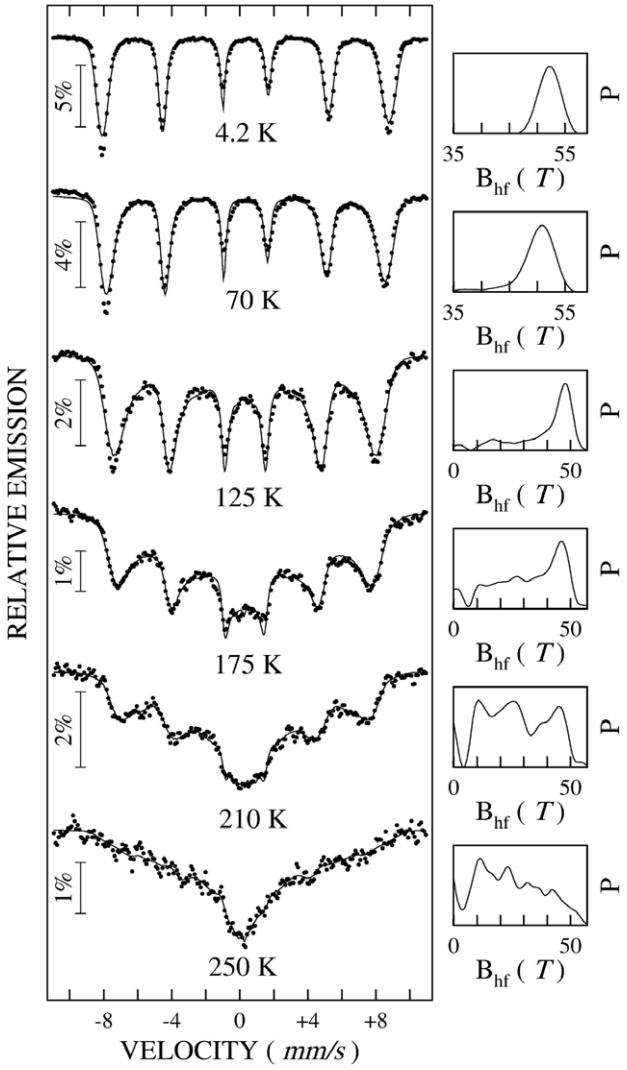

Figure 7. Mössbauer spectra of sample S4 measured at various temperatures. The probability distribution of the hyperfine magnetic filed is shown on the right side. A much faster magnetic relaxation process is evident from these spectra as compared with those of samples S1 to S3.

temperature, T_B, either as the temperature corresponding to the inflection point of the T-dependence of the average magnetic hyperfine field $\langle B_{hf} \rangle$ (alternative 'a'), or as the temperature where the width of the hyperfine field distribution $P(B_{hf})$ reaches its maximum (alternative 'b'). An average of the two temperatures can be considered for a better approximation of the blocking temperature determined by Mössbauer spectroscopy.

The hyperfine field distributions, $P(B_{hf})$, of the temperature dependent Mössbauer spectra presented in figures 4–7 are shown on the right side of the corresponding figure. For samples S1–S3 at low temperatures, the pronounced distribution peak centred at a high hyperfine field becomes broader and moves towards lower fields at higher temperatures (up to 230 K), where an additional weak component also appears in the low field part of $P(B_{hf})$. This additional low field component in $P(B_{hf})$ corresponds to the fast relaxing central component in the Mössbauer spectra and was interpreted as due to a small percentage (10–15%, as resulting from the Mössbauer relative spectral area) of nanoparticles of much lower size than the rest of particles in the sample. By contrast, extremely broad distributions over a wide range of B_{hf},

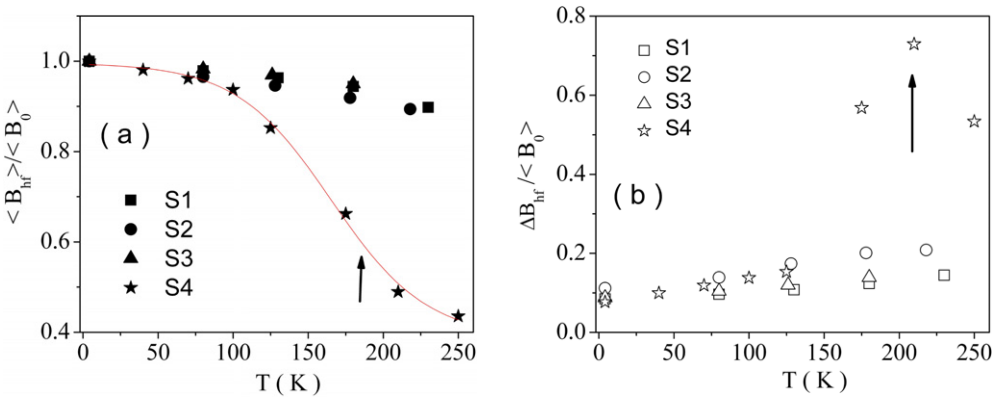

Figure 8. (a) The temperature dependence of the reduced mean magnetic hyperfine field, $\langle B_{\rm hf}\rangle/\langle B_0\rangle$, for samples S1 (squares), S2 (circles), S3 (triangles) and S4 (asterisks). (b) The temperature dependence of the reduced width of the magnetic hyperfine field distribution, $\Delta B_{\rm hf}/\langle B_0\rangle$, for samples S1 (squares), S2 (circles), S3 (triangles) and S4 (asterisks).

including a strong contribution at $B_{\rm hf} = 0$ T, are observed at temperatures higher than 175 K for sample S4 (figure 7), proving a more enhanced magnetic relaxation as compared with samples S1–S3 (figures 4–6). The T-dependences of the reduced mean hyperfine field, $\langle B_{\rm hf}\rangle/\langle B_0\rangle$, and of the reduced distribution width, $\Delta B_{\rm hf}/\langle B_0\rangle$, are presented in figures 8(a) and (b), respectively. It is observed that with the available Mössbauer data a blocking temperature can be defined only for sample S4, with the most pronounced relaxing behaviour at the highest experimental temperatures. A blocking temperature of $T_B = 180$ K can be deduced for sample S4 by following alternative 'a' and of $T_B = 210$ K by following alternative 'b'. An average value of $T_B = 195$ K will be finally considered. It is worth mentioning that due to the incomplete collapse of the Mössbauer spectrum of sample S4 at 250 K higher errors are expected in the estimation of $T_{\rm B}$ via alternative 'a' (the plateau of low fields is not reached, figure 8(a)) than with alternative 'b' (the maximum of the distribution width is well developed, figure 8(b)). Once we know $T_{\rm B}$ for sample S4, additional information on the magnetic anisotropy energy can be obtained from (6). At $T = T_{\rm B}$, $\tau = \tau_M$ and (6) becomes

$$\tau_M = \tau_0 \exp(KV/k_{\rm B}T_{\rm B}). \tag{7}$$

τ_0 depends on the material and is slightly dependent on temperature, and the reported values for τ_0 are spread out in the range from 10^{-13} to 10^{-9} s [17–22]. Using values of $\tau_M = 5 \times 10^{-9}$ s and $\tau_0 = 10^{-11}$ s a magnetic anisotropy energy KV of about 0.17×10^{-19} J can be deduced for this sample. However, this is only a crude estimation of the anisotropy energy due to the uncertainty in τ_0. Conversely, (7) can be more useful for the determination of the right value of τ_0, when adequate information about the blocking temperature and the anisotropy energy is available.

3.4. Determination of the magnetic anisotropy energy and particle size dispersion

In the following, we present a detailed analysis of the magnetic anisotropy energy and of the involved magnetic features in the four ferrofluid samples by using the regime of collective excitations. A quasi-linear decrease of the reduced mean hyperfine field can be observed in the data presented in figure 8(a) for temperatures lower than 175 K in samples S1–S3 and lower than 125 K for sample S4. The decreases of both the reduced mean magnetic hyperfine field

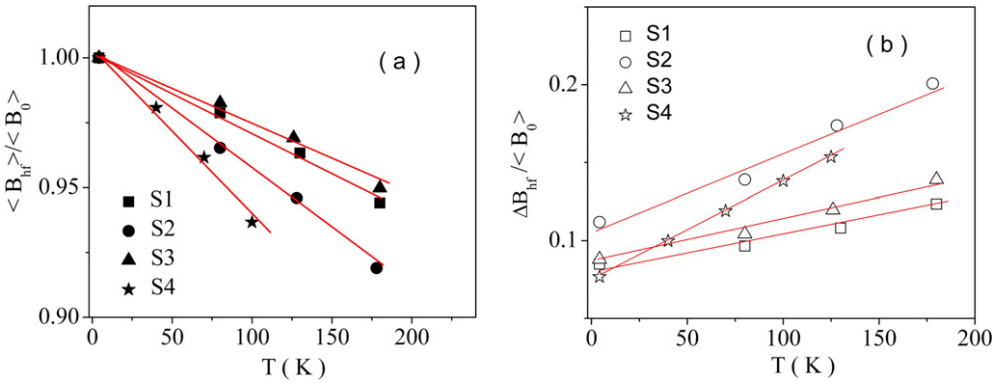

Figure 9. (a) The temperature dependence of the reduced mean magnetic hyperfine field, $\langle B_{\rm hf}\rangle/\langle B_0\rangle$, versus temperature, in the range of its linear decrease, for samples S1 (squares), S2 (circles), S3 (triangles) and S4 (asterisks). The linear fittings providing the slopes SL_1 are also presented. (b) The temperature dependence of the reduced width of the magnetic hyperfine field distribution, $\Delta B_{\rm hf}/\langle B_0\rangle$, in the range of its linear increase, for samples S1 (squares), S2 (circles), S3 (triangles) and S4 (asterisks). The linear fittings providing slopes SL_2 are also presented.

Table 3. The slopes SL_1 and SL_2 of the linear T-dependences of the reduced mean hyperfine magnetic field $\langle B_{\rm hf}\rangle/\langle B_0\rangle$ and the reduced distribution width $\Delta B_{\rm hf}/\langle B_0\rangle$, respectively, and the corresponding anisotropy energy KV and relative size dispersion ($\delta D/D$), for samples S1–S4. The anisotropy constant K and the magnetic diameter, D_M, estimated from the anisotropy energy KV, considering alternatively either the mean diameter obtained by XRD, or the anisotropy constant for the bulk material, are also presented. Numbers in brackets indicate errors of the last digit.

Sample	$-SL_1$ (10^{-5} K^{-1})	SL_2 (10^{-5} K^{-1})	$\delta D/D$	KV (10^{-19} J)	K [a] (10^5 J m^{-3})	D_M [b] (nm)
S1	30(2)	25(2)	0.28(2)	0.23	0.41(5)	∼6
S2	45(2)	50(2)	0.32(2)	0.15	0.16(5)	∼13
S3	25(2)	27(2)	0.33(2)	0.28	0.38(5)	∼7
S4	63(2)	65(2)	0.34(2)	0.11	0.15(5)	∼12

[a] The anisotropy constants, K, were evaluated by considering the physical diameters presented in table 2. The obtained values are substantially lower than the typical anisotropy constant for bulk cobalt ferrite (1.8×10^5 J m^{-3}) [15].
[b] The magnetic diameters, D_M, were estimated by considering anisotropy constants typical for bulk cobalt ferrite (1.8×10^5 J m^{-3}) and bulk magnetite (0.12×10^5 J m^{-3}) [15].

and the reduced distribution width are displayed over the low-T regime in figures 9(a) and (b), respectively. The magnetic anisotropy energy, KV, of each sample was estimated from the slope, SL_1, of the linear fitting of the experimental points in figure 9(a), according to (5):

$$SL_1 = -\frac{k_{\rm B}}{2KV}. \tag{8}$$

The obtained slopes and the corresponding anisotropy energies are given in table 3.

The increase of the reduced distribution width $\Delta B_{\rm hf}/\langle B_0\rangle$ with temperature (figure 9(b)) was interpreted as follows. The nanoparticles with diameter D in the ferrofluid are characterized by a size distribution, $P(D)$ (e.g. a lognormal or a Gaussian distribution). The hyperfine fields of particles with different diameters within the size distribution will follow their own decrease versus temperature, according to (5). Therefore, the increasing width of the hyperfine field distribution, $\Delta B_{\rm hf}$, with rising temperature should be correlated with the different variation of the hyperfine fields for particles of different sizes. Mathematically this

corresponds to the differentiation of equation (5) with respect to the particle diameter, D. It can be shown that for a system of spherical nanoparticles $\Delta B_{\rm hf}/\langle B_0\rangle$ can be expressed as (appendix)

$$\Delta B_{\rm hf}/\langle B_0\rangle = 3\frac{k_{\rm B}}{2KV}\frac{\delta D}{D}T. \tag{9}$$

According to equation (9), the relative width of the hyperfine field distribution, $\Delta B_{\rm hf}/\langle B_0\rangle$, increases linearly with the temperature, with a slope, SL_2, that depends only on the relative width of the particle size distribution, $\delta D/D$ (the relative size dispersion), and on the slope, SL_1:

$$SL_2 = 3\frac{k_{\rm B}}{2KV}\frac{\delta D}{D} = -3SL_1\frac{\delta D}{D}. \tag{10}$$

Equation (10) demonstrates that the relative size dispersion of the particles can be obtained from the slopes SL_1 and SL_2, which are pure Mössbauer experimental results. The experimental results shown in figure 9(b) agree with the predicted linear increase of the relative width of the hyperfine field distribution with temperature, and they provide information about the slope SL_2 for each sample. The slopes SL_1 and SL_2 obtained by the least-square fitting of the Mössbauer data as well as the relative size dispersion $\delta D/D$ for each nanoparticle system are presented in table 3. Concerning the two slopes SL_1 and SL_2, the four samples have to be divided in two different groups: samples S1 and S3 (based on cobalt ferrite) and samples S2 and S4 (based on magnetite particles). For the ferrofluids with cobalt ferrite particles, the magnitude of both slope SL_1 and slope SL_2 is smaller than that of the ferrofluids with magnetite particles, in such a way that their ratio is almost the same for all samples. Therefore, the relative size dispersion in all samples is almost the same ($\delta D/D$ is about 0.31 on average). On the other hand, the magnetic anisotropy energy is higher for samples S1 and S3 as compared to samples S2 and S4, due to the differences in the magnitudes of the slope SL_1 (see table 3).

The anisotropy constant K corresponding to each sample can be straightforwardly computed by starting from the anisotropy energies KV presented in table 3 and the average physical diameters D presented in table 2 (spherical particles are considered). The corresponding values are shown in table 3. Values of about 0.41×10^5 J m^{-3} and 0.38×10^5 J m^{-3} were obtained for the cobalt ferrite nanoparticles surfacted with double layers of mystric acid and oleic acid, respectively (samples S1 and S3, table 3). Such values are about 4 to 5 times lower than the typical bulk value of about 1.8×10^5 J m^{-3} for cobalt ferrite [15]. The anisotropy constants obtained for the magnetite particles (samples S2 and S4, table 3) are almost independent of the type of surfactant and approach, in the error limit, the value of bulk magnetite, 0.12×10^5 J m^{-3} [15]. The significant deviations of the obtained anisotropy constants from their bulk values, for the cobalt ferrite case, cannot be explained by the possible slight variation of the anisotropy constant with the particle size (see [15]) or with the used surfactant. Therefore, a more realistic explanation of the relatively small KV product, in conditions of anisotropy constant values only slightly different from the bulk values, seems to be the formation of a magnetic dead layer at the particle surface, with a thickness that is dependent on the ferrite–surfactant combination. The magnetic dead layer can be understood either as a layer with paramagnetic behaviour or as a layer with randomly oriented spins (e.g. as in a spin-glass-like structure), giving no contribution to the overall particle magnetic moment. The good crystalline state of the samples, proven by XRD, rather sustains the spin-glass-like structure, but new experiments are required in order to clarify this aspect. The magnetic diameter, D_M, corresponds to the magnetic active core of the particle ($D_M = D - 2d$, with D the physical diameter and d the thickness of the magnetic dead layer). It can be

straightforwardly computed from the anisotropy energy KV (given in table 3) and the bulk anisotropy constants for cobalt ferrite and magnetite. The volume V in the expression of the anisotropy energy represents the magnetic volume. The anisotropy constant can vary slightly with the particle size and represents the main source of errors for the estimation of the magnetic volume and, hence, of the magnetic diameter, presented also in table 3. Magnetic diameters of about 6–7 nm are obtained for the cobalt ferrite particles (samples S1 and S3) and of 12–13 nm for magnetite particles (for samples S2 and S4 the magnetic diameter coincides in the error limit with the physical one). Consequently, a negligible magnetic dead layer d is estimated for the magnetite particles and a magnetic dead layer of about 2 nm for the cobalt ferrite particles.

Finally, the time constant τ_0 can be calculated for sample S4, for which both the blocking temperature and the anisotropy energy were deduced only via Mössbauer spectroscopy. A value of about 8×10^{-11} s is obtained by introducing $\tau_M = 5 \times 10^{-9}$ s, $T_B = 195$ K and $KV = 0.22 \times 10^{-19}$ J in equation (7). It is worth mentioning that τ_0 can also be obtained from the different T_B values measured by SQUID magnetometry and Mössbauer spectroscopy on the same sample [22]; however, in this case errors in the time windows of both techniques are involved.

4. Conclusions

Ferrofluids consisting of cobalt ferrite and magnetite nanoparticles double coated with different surfactants and dispersed in water were prepared and subsequently characterized by XRD and Mössbauer spectroscopy. The XRD data provide proof of the crystalline state and yield average physical diameters of about 11 nm for all nanoparticle systems.

Mössbauer spectroscopical results obtained at 4.2 K in zero external field support a correct site occupation in the inverse spinel structure of the both ferrites. The temperature-dependent Mössbauer data reveal the most pronounced magnetic relaxation behaviour for the sample prepared with magnetite and double coated with lauric acid surfactant. The blocking temperature in this system was estimated to be about 195 K, by employing two alternative procedures which are based on the temperature evolution of the magnetic hyperfine field distribution. The time constant τ_0 in the Néel formula for superparamagnetic relaxation was estimated purely from Mössbauer spectroscopy data in zero external field.

Information on both the relative size dispersion of the particles and their magnetic anisotropy energy were obtained from the Mössbauer spectra in the temperature regime of collective excitations. The results support the formation of a magnetic dead layer at the surface of the nanoparticles, whose thickness is strongly dependent on the ferrite type and slightly dependent on the surfactant type. Dead layers of negligible thicknesses were estimated for the magnetite particles and of about 2 nm for the cobalt ferrite particles. Hence, the much higher crystalline magnetic anisotropy constant of the cobalt ferrite (as compared with the anisotropy constant of magnetite) cannot improve substantially the magnetic performances of the cobalt-ferrite based ferrofluids at ambient temperature. The use of an inappropriate surfactant for magnetite particles could enhance substantially the superparamagnetic relaxation behaviour, leading to a low saturation magnetization of such ferrofluids at ambient temperature.

Acknowledgments

We are grateful to U von Hörsten (Duisburg) for expert technical assistance and discussions. The work at Duisburg was supported by the Deutsche Forschungsgemeinschaft (SFB 491) and at Bucharest by the CEEX NanoMagneFluidSeal project.

Appendix

The derivative of equation (5) with respect to the particle size, D, gives

$$\frac{\mathrm{d}B_{\mathrm{hf}}}{\mathrm{d}D} = -B_0 \frac{k_{\mathrm{B}}T}{2K}\frac{\mathrm{d}}{\mathrm{d}D}\left(\frac{1}{V}\right) = B_0 \frac{k_{\mathrm{B}}T}{2KV}\frac{1}{V}\frac{\mathrm{d}V}{\mathrm{d}D}. \tag{A.1}$$

Assuming nanoparticles with regular shapes (e.g. spheric or cubic), the volume can be expressed as $V = \xi D^3$ (with ξ a proportionality constant depending on the particle shape).

In this case equation (A.1) can be expressed as

$$\frac{\mathrm{d}B_{\mathrm{hf}}}{\mathrm{d}D} = B_0 \frac{k_{\mathrm{B}}T}{2KV}\frac{3}{D} \tag{A.2}$$

or, alternatively,

$$\frac{\mathrm{d}B_{\mathrm{hf}}}{B_0} = \frac{3k_{\mathrm{B}}T}{2KV}\frac{\mathrm{d}D}{D}. \tag{A.3}$$

Therefore, the width of the hyperfine field distribution, ΔB_{hf}, will be connected to the width of the particle size distribution, δD, via the relation

$$\frac{\Delta B_{\mathrm{hf}}}{B_0} = 3\frac{k_{\mathrm{B}}}{2KV}\frac{\delta D}{D}T. \tag{A.4}$$

References

[1] Popplewell J 1984 *Phys. Technol.* **15** 150
[2] Bailey R L 1983 *J. Magn. Magn. Mater.* **39** 178
[3] Odenbach J 2004 *J. Phys.: Condens. Matter* **16** 1135
[4] Orlov L P and Fertman V E 1980 *Magnetohydrodynamics* **164** 400
[5] Odenbach S 2000 *Int. J. Mod. Phys.* B **14** 1615
[6] Vadasz J V, Govender S and Vadasz P 2005 *Int. J. Heat Mass Transfer* **48** 2673
[7] Roger J, Pons J N, Massart R, Halbreich A and Bacri J C 1999 *Eur. Phys. J.* AP **5** 321
[8] Halbreich A, Groman E V, Raison D, Bouchaud C and Paturance S 2002 *J. Magn. Magn. Mater.* **248** 276
[9] Prasad M K, Panda D, Singh S, Mukadam M D, Yusuf S M and Bahadur D 2005 *J. Appl. Phys.* **97** 10Q903
[10] Sem S, Manciu M and Manciu F S 1999 *Appl. Phys. Lett.* **75** 1479
[11] Yu Zubarev A and Yu Iskakova L 2004 *Physica* A **343** 65
[12] Vekas L, Bica D, Marinica O, Rasa M, Socoliuc V and Stoian F D 2005 *J. Magn. Magn. Mater.* **289** 50
[13] Brand R A 1987 *Nucl. Instrum. Methods Phys. Res.* B **28** 398 the NORMOS program is available from WISSEL GmbH, D-82319 Starnberg, Germany
[14] Suryanarayana C and Grant Norton M 1998 *X-ray Diffraction; A Practical Approach* (New York: Plenum)
[15] Brabes V A M 1995 *Handbook of Magnetic Materials* ed K H J Buschow (Amsterdam: North-Holland)
Bickford L R 1950 *Phys. Rev.* **78** 449
Tung L D, Kolesnichenko V, Caruntu D, Chou N H, O'Connor C J and Spinu L 2003 *J. Appl. Phys.* **93** 7486
Rondinone A J, Samia A C S and Zhang Z J 2000 *Appl. Phys. Lett.* **76** 3624
[16] Greenwood N N and Gibb T C 1971 *Mössbauer Spectroscopy* (London: Chapman and Hall)
[17] Thomas M F and Johnson C E 1986 *Mössbauer Spectroscopy* ed D P E Dickson and F J Berry (Cambridge: Cambridge University Press)
[18] Morup S 1983 *J. Magn. Magn. Mater.* **37** 39
[19] Neel L 1949 *Ann. Geophys.* **5** 9
[20] Campbell S J and Gleiter H 1993 *Mössbauer Spectroscopy Applied to Magnetism and Material Science* vol 1, ed G J Long and F Grandjean (New York: Plenum)
[21] Dormann J L, Fiorani D and Tronc E 1997 *Advances in Chemical Physics* vol XCIII, ed I Prigogine and A Rice (New York: Wiley)
[22] Chien C L 1991 *J. Appl. Phys.* **69** 5267